# Thermal-Hydraulic Study of the LBE-Cooled Fuel Assembly in the MYRRHA Reactor: Experiments and Simulations

**J. Pacio*, T. Wetzel**
Karlsruhe Institute of Technology (KIT) – Institute of Nuclear and Energy Technologies (IKET)
Hermann-von-Helmholtz Platz 1, D-76344 Eggenstein-Leopoldshafen, Germany
julio.pacio@kit.edu, thomas.wetzel@kit.edu

**H. Doolaard, F. Roelofs**
Nuclear Research and Consultancy Group (NRG), Westerduinweg 3, Petten, the Netherlands
doolaard@nrg.eu, roelofs@nrg.eu

**K. Van Tichelen**
Belgian Nuclear Research Center (SCK•CEN), Boeretang 200, Mol, Belgium
kvtichel@sckcen.be

## ABSTRACT

Heavy liquid metals (HLMs), such as lead-bismuth eutectic (LBE) and pure lead are prominent candidate coolants for many advanced systems based on fast neutrons. In particular, LBE is used in the first-of-its-kind MYRRHA fast reactor, to be built in Mol (Belgium), which can be operated either in critical mode or as a sub-critical accelerator-driven system. With a strong focus on safety, key thermal-hydraulic aspects of these systems, such as the proper cooling of fuel assemblies, must be assessed. Considering the complex geometry and low Prandtl number of LBE (Pr~0.025), this flow scenario is challenging for the models used in Computational Fluid Dynamics (CFD), e.g. for relating the turbulent transport of momentum and heat. Thus, reliable experimental data for the relevant scenario are needed for validation.

In this general context, this topic is studied both experimentally and numerically in the framework of the European FP7 project SEARCH (2011-2015). An experimental campaign, including a 19-rod bundle with wire spacers, cooled by LBE is undertaken at KIT. With prototypical geometry and operating conditions, it is intended to evaluate the validity of current empirical correlations for the MYRRHA conditions and, at the same time, to provide validation data for the CFD simulations performed at NRG. The results of one benchmarking case are presented in this work. Moreover, this validated approach is then used for simulating a complete MYRRHA fuel assembly (127 rods).

**KEYWORDS**
LBE, experiment, validation, MYRRHA, rod bundle

## 1. INTRODUCTION

In several next-generation nuclear systems, particularly in fast-reactors and accelerator-driven systems, liquid metals (LMs), such as sodium and lead (alloys), are considered as primary coolants. The innovative MYRRHA reactor, see section 2, uses the lead-bismuth eutectic alloy LBE. For the further development

* Corresponding author. Tel: +49 721-60826902

of these systems, with a focus on inherent safety, several thermal-hydraulics issues must be investigated in detail, particularly by providing and evaluating experimental data for the validation of available predicting models. This work is focused on the thermal-hydraulics of core sub-assemblies in the MYRRHA reactor, in a broad range of operating conditions.

The study of this thermal-hydraulic scenario presents several challenges. First, due to their particularly low Prandtl number of LBE ($Pr=c_p\ \mu\ \lambda^{-1} \sim 0.025<<1$), the molecular diffusion of heat is much larger than that of momentum. Thus, even at large Reynolds number (Re), the molecular thermal diffusivity plays a large role, affecting the statistical behavior of the velocity and temperature profiles in turbulent flows; see e.g. [1]. Thus, turbulence models based on the Reynolds analogy ($Pr_t=1$), commonly used for water or air ($Pr>\sim1$) are not applicable, and specific models are required.

Second, fuel assemblies have a rather complex geometry, particularly considering the presence of spacing elements. Figure 1 shows a diagram of a hexagonal bundle with one wire spacer around each rod, as considered in this work. Many parameters are needed for representing this geometry, as indicated in Figure 1, in addition to the number of rings (n) and rods (N). Three different types of sub-channels are defined: internal, edge and corner; i.e. surrounded by 3, 2 or 1 rods, respectively. They present a different hydraulic diameter $d_h$ and thermal boundary condition: the rods are heated, while the duct walls are not. Furthermore, depending on the axial position, some of them are partially obstructed by the wires.

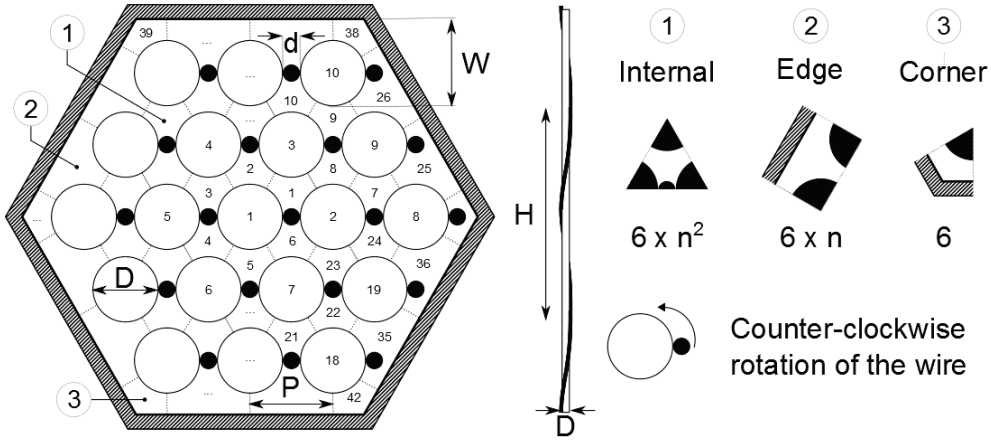


**Figure 1. Schematic representation of a rod bundle with wire spacers. "n" is the number of rings, in this case n=2.**

Third, only limited experimental information is currently available for this scenario. Due to the typically large average heat transfer coefficients ($\alpha$) in LMs, large wall heat flux densities ($q_w$) are needed in order to attain temperature differences which can be accurately measured. This condition strongly affects the design of the experimental setup and the instrumentation, given the limited space and steep gradients.

This topic has been extensively studied previously, in the framework of national LMFBR programs. A review of previous investigations in bare hexagonal bundles can be found e.g. in [2]. Furthermore, design-specific heat transfer tests of fuel assembly mockup using sodium were performed in the past [3-7], supported by mockup tests with water and air. Some valuable lessons can be learned from these previous experiences. In particular, empirical correlations have been developed for the main engineering parameters: friction coefficient (f) and Nusselt number (Nu).

An extensive database of pressure-drop data has been collected throughout the years and several correlations have been proposed. In a recent review [8] their predicting performance was compared and the best results were obtained by the correlation of Cheng and Todreas [9], which considers three regimes depending on Re and the pitch-to-diameter ratio (P/D).

All available correlations for the Nusselt number are based on experimental data for bundles *without* spacers, as reviewed by [2]. The wire spacers affect the flow, leading to a directional sweeping, and increased turbulent mixing, although they partially obstruct the cross flow between sub-channels. Thus, this scenario presents more three-dimensional effects which can locally enhance or diminish the mean heat transfer coefficient. In the absence of more specific models, these correlations are considered for comparison in the present work. They express the Nusselt number (Nu) as a function of the Péclet number (Pe=Re*Pr) and the P/D ratio. Two specific correlations are considered. The model by Ushakov et al [10], given by eq. (1), is recommended in [11] for P/D>1.3.

$$Nu = 7.55\ P/D - 20\ (P/D)^{-13} + 3.67\quad (P/D)^{-2}\ Pe^{(0.56+0.19\ P/D)} / 90 \tag{1}$$

Moreover, the model by Kazimi and Carelli [12], given by eq. (2), is the most conservative prediction.

$$Nu = 4.0 + 0.16\ (P/D)^{5.0} + 0.33(P/D)^{3.8}\ (Pe/100)^{0.86} \tag{2}$$

This work is performed at three institutions as part of the European FP7 project SEARCH (2011-2015). In cooperation with the MYRRHA team at SCK-CEN (Belgium), this topic is studied experimentally at KIT (Germany) and numerically at NRG (Netherlands).

## 2. THE MYRRHA REACTOR AND ITS FUEL ASSEMBLY DESIGN

MYRRHA is a multipurpose fast neutron spectrum irradiation facility under design at SCK•CEN [13], proposed to operate as a European large research infrastructure and to serve as European Technology Pilot Plant for the Lead Cooled Fast Reactor [14]. Furthermore, MYRRHA is proposed to serve as a technological system for waste transmutation demonstration and as an irradiation facility for material and fuel in support of the liquid metal fast reactor systems.

In this unique design, MYRRHA is conceived as an accelerator driven system (ADS), able to operate in sub-critical and critical modes. It contains a proton accelerator of 600 MeV, a spallation target and a multiplying core with MOX fuel, cooled by liquid Lead-Bismuth Eutectic (LBE).

The fuel assembly design is similar to a typical design used in fast spectrum reactors cooled by liquid sodium [15]. The MYRRHA fuel assembly contains a hexagonal bundle of cylindrical fuel rods surrounded by a hexagonal shroud or wrapper (see Figure 2). The upper and lower ends of the shroud are connected to the inlet and outlet nozzles guiding the LBE coolant through the fuel assembly.

This fuel bundle is composed of a central fuel rod surrounded by 6 hexagonal rings of the fuel rods (127 rods in total – outer diameter 6.55 mm). Helical wire-spacers wound on the outer surface of each fuel rod keep them separated from one another in the bundle. In the fuel rod design presented in this paper, the helical wire spacer with a diameter of 1.75 mm and a helicoid lead of about 262 mm (pitch/clad diameter=40) are adopted to keep a pitch of 8.4 mm (cold design conditions) between the neighbor fuel pins in the bundle.

A maximum core power of 100 MW is considered. With a critical core configuration of 69 fuel assemblies and taking into account radial peaking factors, average bundle powers and maximum wall heat fluxes as listed in Table 1 are obtained.

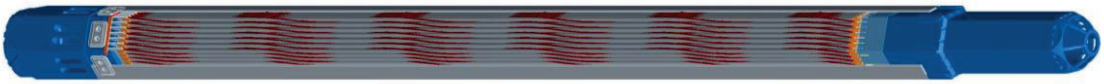

**Figure 2. Side view of MYRRHA fuel assembly. The flow is upward (here from left to right)**

In this work, the thermal-hydraulic study is focused on the heat transfer in the active region.

## 3. EXPERIMENTAL SETUP AT KIT – KALLA

A prototypical experiment is setup at the Karlsruhe Liquid Metal Laboratory (KALLA) of KIT. For this study, the existing LBE loop THEADES is used, with the following maximum parameters. The centrifugal pump yields a flow rate up to 47 $m^3$ $h^{-1}$ (~135 kg $s^{-1}$ at 300°C) and a pressure head of 5.9 bar. A large air cooler with a design capacity of 500 kW is the available heat sink. With an oxygen control system, steady-state operation up to 450°C is possible [16]. Moreover, a filter is placed at the inlet of the test section in order to prevent solid particles from entering the heated zone.

The test section consists of a bundle of 19 electrically-heated rods, embedded in a hexagonal channel, surrounded by unheated, static LBE. A side view of this arrangement is shown in Figure 3.

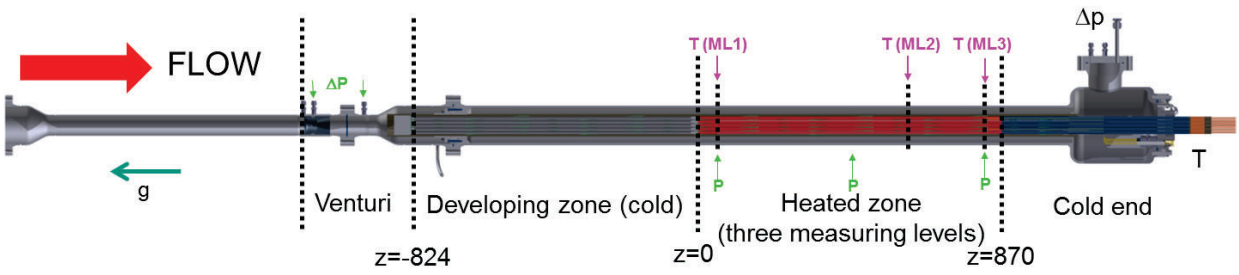


**Figure 3. Schematic side view of the test section. All axial positions are expressed in mm, referred to the onset of the heated zone (z=0).**

In the flow direction (upward), first a Venturi nozzle is installed for supplementing the Vortex flow meter (±0.75%) placed at the outlet, particularly at low velocities. At the transition from round pipe to the hexagonal channel, a pinfixer is placed, keeping the rods in position in parallel rows, following the MYRRHA design. A long cold developing zone is found upstream of the heated section, and a fully-developed velocity profile can be assumed at z=0.

The main dimensions and operating variables of this experiment, listed in Table I, are prototypical of those found in the MYRRHA reactor. In particular, the ratios P/D and H/D are kept constant, while the heating elements are up-scaled for practical reasons. Two hydraulic diameters are considered: $d_{h,bdl}$ (bundle) for the pressure-drop analysis and $d_{h,sch}$ (internal sub-channel) for the heat-transfer study.

**Table I. Main geometrical parameters and operating conditions of both setups, compared to the fuel assembly of the MYRRHA reactor**

| Mesh | Symbol, | KIT–KALLA | MYRRHA | Ratio |
|---|---|---|---|---|
| **Number of rods** | N, - | 19 | 127 | |
| **Rod diameter** | D, mm | 8.20 | 6.55 | 1.25 |
| **Rod heated length** | $L_{heat}$, mm | 870 | 600 | 1.45 |
| **Rod upstream unheated length** | $L_{cold}$, mm | 820 | 660 | 1.24 |
| **Pit-to-diameter ratio** | P/D, - | 1.279 | 1.279 | 1 |
| **Wire spacer diameter** | d, mm | 2.20 | 1.75 | 1.25 |
| **Wire axial pitch** | H, mm | 328 | 262 | 1.25 |
| **Hydraulic diameter – bundle** | $d_{h,bdl}$, mm | 5.20 | 4.01 | 1.29 |
| **Hydraulic diameter – subchannel** | $d_{h,sch}$, mm | 4.74 | 3.79 | 1.25 |
| **Bulk temperature** | T, °C | 200 – 450 | 270 – 410 | |
| **Thermal power per bundle** | Q, kW | 39 – 433 | 1449 | |
| **Wall heat flux density** | $q_w$, kW $m^{-2}$ | 92.5 – 1016 | 92.5 – 1378 | ~1 |
| **Mass flow rate per bundle** | $\dot{m}$, kg $s^{-1}$ | 1.12 – 19.2 | 5.0 – 71.4 | |
| **Reynolds number ($Re=\rho\ u\ d_{h,sch}\ \mu^{-1}$)** | Re, - | 2100 – 63100 | 2600 – 48000 | ~1 |
| **Péclet number ($Pe=\rho\ u\ d_{h,sch}\ c_p\ \lambda^{-1}$)** | Pe, - | 54 – 1258 | 58 – 955 | ~1 |

With three probes located at z = 54.5, 437.5 and 820.5 mm, two values of differential pressure are obtained within the bundle. In all cases, lines filled with LBE (along the gap between both vessels) are used for connecting the measuring points to the sensors, placed at a single horizontal level (Rosemount 3051 DP transmitters, set to an accuracy of ±0.47 mbar). All offsets (including the hydrostatic term) are removed by setting the signals to zero in isothermal tests without flow. Moreover, thermocouples (TCs) are placed at selected axial positions in order to correct for the temperature-dependent changes in density.

In total 80 TCs (type K, steel jacket) are used in this experimental campaign. One TC is placed at the inlet and three at the outlet (a mean value is obtained, considering a possibly incomplete mixing), for indicating $T_{in}$ and $T_{out}$, respectively. Seven TCs are placed at the pressure lines (PLs), as described above. The remaining 69 TCs are distributed at the three measuring levels (MLs) defined in the heated zone, see Figure 3. These are selected considering the local azimuthal position of the wires, which rotate 60° in an axial distance of H/6. Thus, at exact multiples of H/6, identical 60°-sectors can be identified. This geometrical feature is exploited for the instrumentation, defining the three MLs at z= 54.6, 601.3 and 820 mm (z/H=1/6, 11/6 and 15/6). At each ML, five TCs (0.25 mm) are installed at the center of selected sub-channels (A to E), marked as red squares in Figure 4. Seven TCs (0.5 mm) are placed at the walls facing those sub-channels (A to E), marked as green diamonds in Figure 4. Allowing for a maximum of three wall TCs at each heated rod (they are placed in grooves in the steel cladding), additional 11 wall TCs are placed at each ML. These include three locations behind the wires (rods #11, #15 and #19).

All TCs are calibrated simultaneously, in isothermal tests with large flow rates, and using $T_{in}$ as a reference, leading to a relative precision of ±0.1 K, that is much better than the absolute accuracy reported by the manufacturer (1.5 K). Furthermore, given that the wall TCs are located inside the cladding, the observed value is larger than the temperature at the outer surface. For LM experiments, this systematic overestimation can be significant, see e.g. [17]. Considering a temperature gradient proportional to $q_w$ (thermal conduction through the wall), a correction is applied in order to avoid systematic errors.

After confirming a valid heat balance in the test section, the experimental value of Q (and $q_w$) is given by the measured applied electrical power (±1%). Considering a uniform heat flux distribution and a constant heat capacity, the local bulk temperature $T_b(z)$ is linearly interpolated between $T_{in}$ and $T_{out}$.

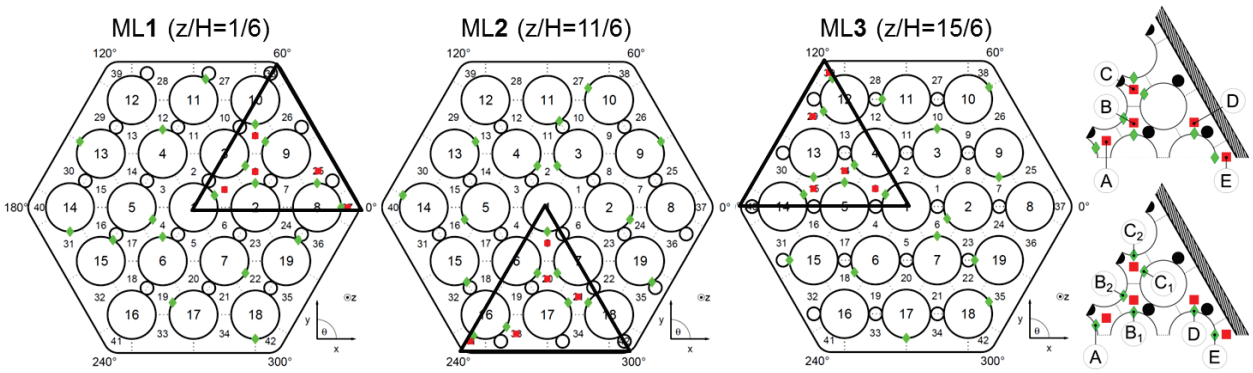


**Figure 4. Distribution of the TCs in the three measuring levels (MLs). At each ML, 5 TCs are installed in the sub-channels (red squares) and 18 TCs at the wall (green diamonds).**

## 4. RESULTS FOR A REFERENCE CASE

The complete test matrix considers 78 experimental cases, covering a broad range of operating conditions, as listed in Table I. This section focuses on the results for one reference case, whose operating conditions are $\dot{m}$=(15.97±0.14) kg $s^{-1}$, Q=(197±1.97) kW and $T_{in}$=(200.1±0.1) °C. These correspond to the same nominal Reynolds number as in the MYRRHA fuel assembly, and 50% of the heat flux density $q_w$.

Figure 5 shows the observed temperature profiles at each ML, in terms of $T-T_b$ (z).

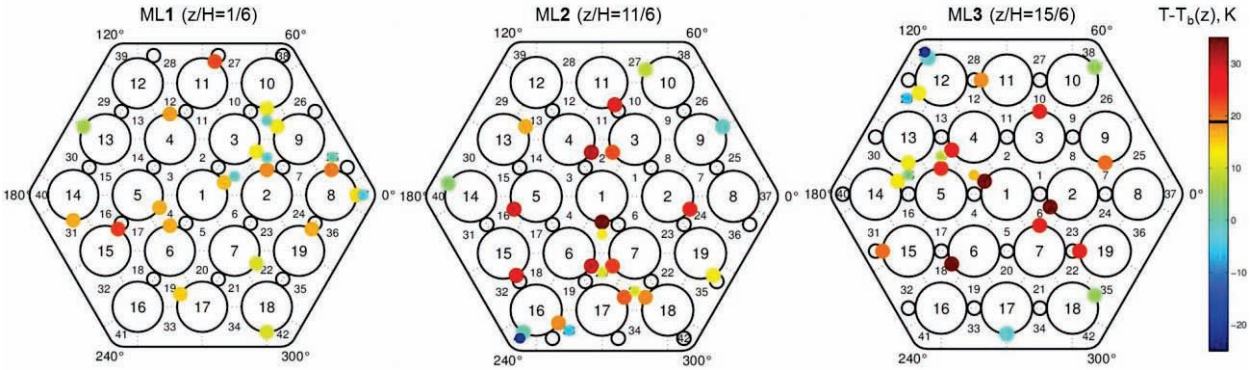


**Figure 5. Local temperature profiles ($T-T_b$) at each ML for a reference case. The solid line indicates the mean wall temperature overheat: $T_{w,m}-T_b$ = 18.8 K at ML3**

Several general trends can be observed in Figure 5. First, the inner regions of the bundle are hotter than the outer ones, as a consequence of a lower heating and higher velocity at the edges. Second, a similar temperature (around or below $T_b$) is measured in all sub-channels at ML1, indicating that the heat diffusion from the wall to the sub-channel center is not completely developed and the center is thus relatively cold at this axial position. Third, relatively hot spots are observed behind the wires (rods #11, #15 and #19), particularly at ML1.

The evolution of these general trends can be better understood considering the measurements at the selected locations A to E in the identical sectors (see Figure 4). These are presented in Figure 6, both at the fluid ($T_f-T_b$, left) and at the wall ($T_w-T_f$, right).

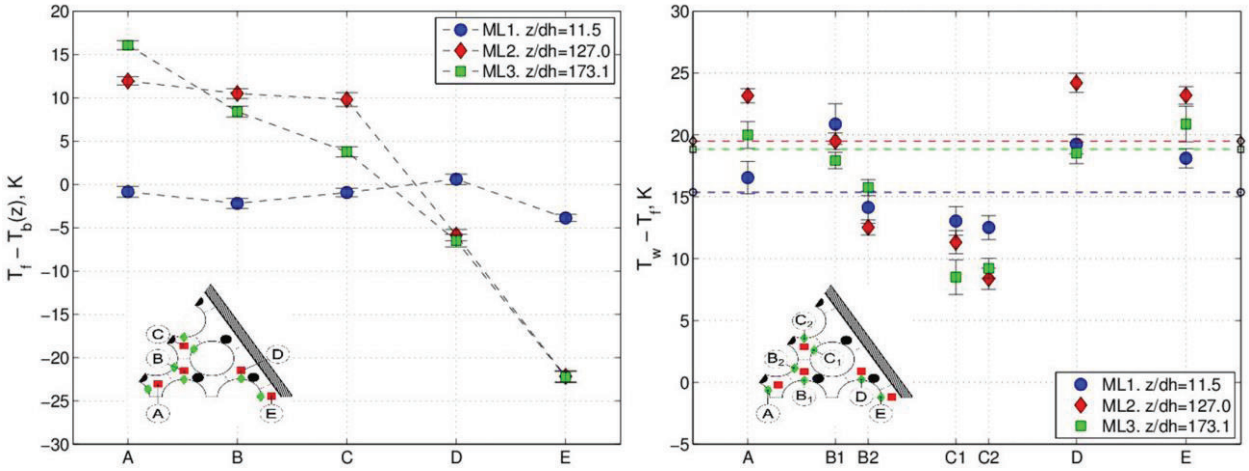


**Figure 6. Evolution of the local temperature differences at the selected locations A to E for the reference case. Left: at the center of the subchannel ($T_f$-$T_b$). Right: overheat at the walls facing those subchannels ($T_w$-$T_f$); the dashed lines indicates the mean wall temperature ($T_{w,m}$-$T_b$)**

As discussed above, a relatively flat fluid temperature profile is observed at ML1, and the inner regions are hotter than the outer ones at ML2 and ML3. At both the edge (D) and corner (E) locations the same results, within the experimental uncertainties, are obtained at ML2 and ML3.

Both global and local effects have to be considered for understanding the wall temperature overheat. Although the mean difference $T_{w,m}$-$T_b$ (dashed lines) remains roughly constant from ML2 to ML3, the distribution continues to develop. At the locations D and E, the local temperature difference $T_w$-$T_f$ is higher than the mean value, because the fluid is relatively cold. Locally, a higher temperature is expected in the proximity of the wire spacers. For example, the location B1 is an angular distance of 30°, and the B2 is at 90° and indeed $T_{B1}$>$T_{B2}$.

## 5. CFD MODEL DEVELOPMENT

Next to operational experience using LBE as coolant, the results presented in the previous section provide validation data for a Computational Fluid Dynamics (CFD) modeling. The complex mixing in wire wrapped fuel assemblies and the low Prandtl number of LMs are two of the challenging aspects for such codes and models as described elaborately in [15, 18]. Specially, experimental validation is lacking up to now. Therefore, the experiments conducted in the KALLA laboratory provide unique data for the validation of CFD approaches.

The wire shape is simplified in order to facilitate the meshing, according to the wire shape study of [19], as in Figure 7. The mesh resolution in the fluid is similar to the finest mesh of [19], providing mesh-independent results, and a boundary layer is added to the wires. The cross section of the wire and the smallest distance between the wire and the next rod is the same as for the real wire.

In this work, the commercial code STAR-CCM+ is used for the modeling and a polyhedral mesh with hexagonal boundary layer is created. The SST k-ω is applied with second order schemes, which is shown to provide accurate results for geometry-dominated liquid metal flows in wire wrapped rod bundles [20]. The default turbulent Prandtl number of 0.9 is applied. The authors are aware that there are currently more sophisticated heat transfer models under development which are dedicated to liquid metals (e.g. [22]). However, these models were not implemented and validated at the moment of simulating. All

residuals have decreased at least 3 orders of magnitude at convergence, which is confirmed by temperature convergence at representative monitor points. Temperature-dependent properties of LBE are taken from [11], see Appendix A.

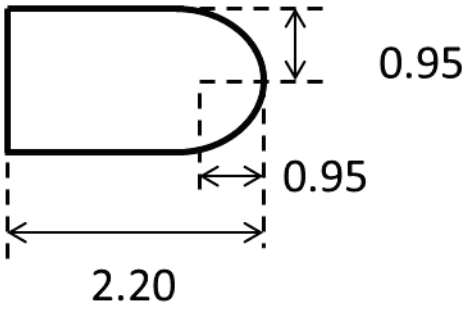


**Figure 7. Approximate wire shape for the numerical simulations (all units are given in mm)**

Two different CFD models are used in this work, as described in Table II. The first one, including conjugate transfer in the rods and wires is applied to the analysis of the KALLA test (19 rods), see section 6. This is, however, not practical for the MYRRHA reference case (127 rods), see section 7.

**Table II. Main distinctive features of the two numerical models considered in this work**

| **Mesh** | **Model 1** | **Model 2** |
|---|---|---|
| **Approximate wire shape** | As in Figure 7 | |
| **Inlet boundary condition** | Given $\dot{m}$ and $T_{in}$, uniform velocity profile | |
| **Outlet boundary condition** | Zero pressure | |
| **Conjugate heat transfer** | Yes | No |
| **Applied heat flux** | Uniform at inside cladding | Uniform at outside cladding |
| **Adiabatic walls** | Channel wall | Channel wall and wires |

## 6. SIMULATION RESULTS FOR THE KALLA EXPERIMENT

In order to validate the numerical approach, the computational domain of the CFD model for the 19-pin experimental KALLA bundle contains the steel cladding of the rods, the wires and the fluid part, accounting for the conjugate heat transfer in these steel parts (model 1 in Table II). Since the validation data from the experiment includes mainly temperature measurements, the temperature should be as accurate as possible. It is expected that the conjugate heat transfer in the rods and wires has a larger influence on the temperature distribution than the wire shape as studied in [19].

The operating conditions from the reference case studied in section 4 are considered. The streamwise length of the computational domain is selected to obtain a fully developed flow at the start of the heated section and negligible influence of the outlet boundary conditions on the flow at the third measurement plane. One wire pitch is modeled upstream of the heated section in order to obtain a hydraulically developed flow, which is already obtained after ½ wire pitch as shown in [19]. In total four wire pitches are modeled, leaving about ⅓ wire pitch downstream of the heated section, which is sufficient to avoid influences of the boundary conditions at the outlet at the third measurement plane. These considerations lead to a total mesh size of 159 million cells in the fluid and 43 million in the solid. The average y+ value in the heated section for this validation case is 0.9.

Figures 8 and 9 show velocity and temperature profiles, respectively, for this reference case. The velocity profiles from figure 8 are basically the same for model 1 and 2, since this is a forced flow dominated by the geometry. Figure 9 shows the local wall temperature with respect to the bulk temperature - computed according to the linear interpolation from section 3 - , showing the same trends as in the experiment shown in figure 5.

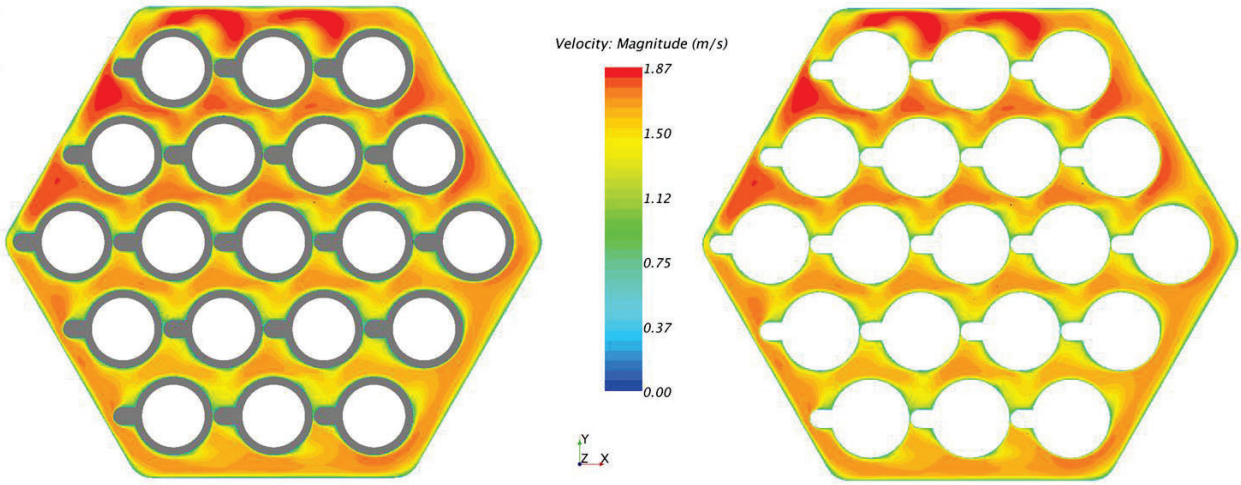


**Figure 8. Calculated velocity profiles for the KALLA reference case, left for model 1 including conjugate heat transfer and right for model 2.**

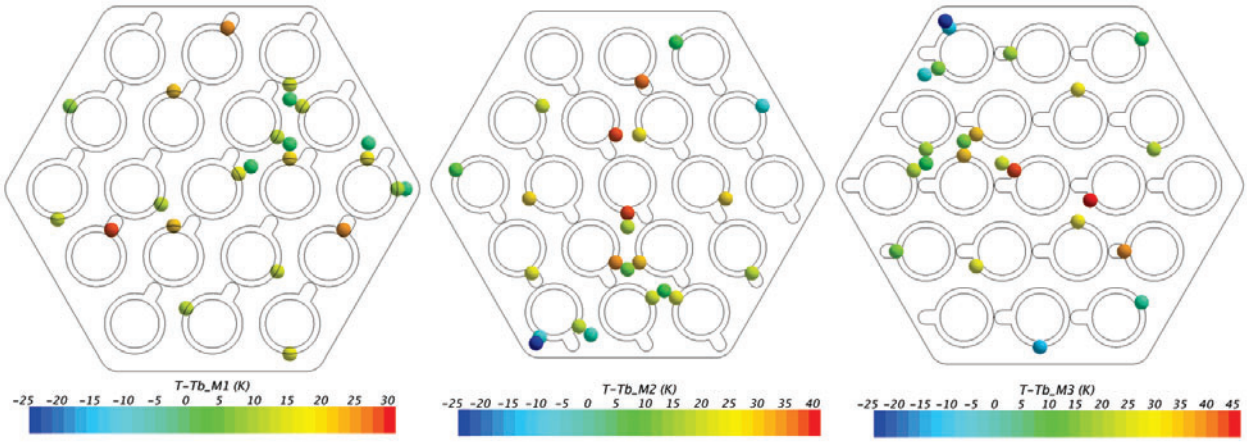


**Figure 9. Local temperature profiles ($T-T_b$) at each ML for the KALLA reference case for model 1.**

Figure 10 shows the fluid temperature and the wall temperature with respect to the bulk temperature at the same thermo-couple positions as in figure 6. The fluid temperature is overestimated with respect to the experiment, but the two simulation models show a good agreement. Although the prediction of the wall temperature shows larger differences, the maximum difference is only 3 °C. It has to be noted that the thermocouples had to be moved slightly into the fluid for model 2 in order to have a measurement point within the domain, since the solids are not taken into account.

Moreover, the results from the experiments and the simulations are summarized in Table III. The comparison with the experiments is focused on the temperature and the heat transfer. The temperatures are probed at the locations of the thermocouples and the same analyses are applied as in the experiments. The Nusselt number is computed from the average wall temperature of all thermocouples and the bulk temperature given from a linear interpolation, see section 3. The pressure difference is computed from the mass flow averaged pressure at the pressure—measurement planes.

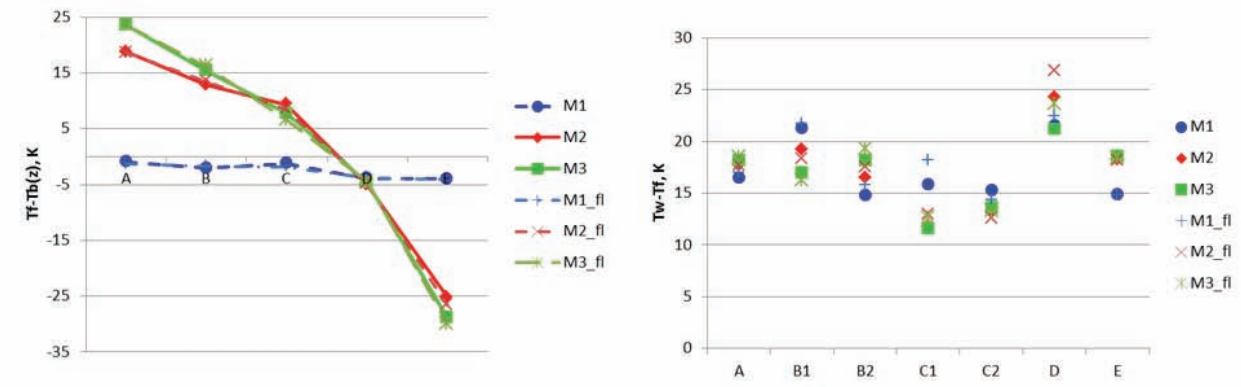


**Figure 10. Evolution of the local temperature differences at the selected locations A to E for the reference case. Left: at the center of the sub-channel ($T_f$-$T_b$). Right: overheat at the walls facing those sub-channels ($T_w$-$T_f$). Model 2 (fluid only) is indicated by the legend Mx_fl.**

**Table III. Comparison of the results for a reference case: experiments, simulations with model 1 and 2 and prediction by empirical correlations**

| Variable | Symbol | Experiment | CFD 1 | CFD 2 | Correlation |
|---|---|---|---|---|---|
| **Pressure difference – sector 1** | $\Delta p_1$, mbar | 211.5±0.7 | 179.2 | 179.4 | 212.8 [9] |
| **Pressure difference – sector 2** | $\Delta p_2$, mbar | 215.5±0.8 | 173.6 | 173.7 | 209.7 [9] |
| **Nusselt number at ML1** | $Nu_1$, - | 13.61±0.86 | 13.02 | 13.71 | 15.4 [10], 10.8 [12] |
| **Nusselt number at ML2** | $Nu_2$, - | 10.02±0.26 | 9.49 | 9.45 | 15.0 [10], 10.4 [12] |
| **Nusselt number at ML3** | $Nu_3$, - | 10.12±0.53 | 9.11 | 8.94 | 14.9 [10], 10.3 [12] |

The pressure drop is under-estimated in the simulations compared to the experiments and the correlations. The difference of about 17 % with the Cheng and Todreas-correlation is similar as observed in other simulations of wire-wrapped rod bundles [21]. The experimental and simulation values of Nusselt are over-predicted by the reference correlation of [10], and are in good agreement with the most conservative predictions from [12]. Overall, the difference between model 1 and 2 is minor, especially at ML2 and ML3 which are of main interest due to the higher temperatures.

## 7. NUMERICAL STUDY OF THE MYRRHA FUEL ASSEMBLY

Due to the large size of this geometry (127 pins), the solid structures are omitted, using the model 2 in Table II. When omitting the rods and the wires, the total heat input is retained while transferring the heat flux boundary condition from the inner cladding surface to the outer cladding surface.

The geometry of the MYRRHA fuel assemblies is summarized in Table I. Considering both the heated and unheated regions, a total mesh size of 9.5 million cells is obtained, applying the reduced resolution meshing approach from [19]. There Gopala et al. showed that the main flow features are still captured, although differences occur e.g. in the pressure drop prediction. For more details, the reader is referred to [19]. A reference case is studied with the following operating conditions: $\dot{m}$=71.4 kg $s^{-1}$, Q=1449 kW and $T_{in}$=270 °C.

Although an inlet header is present in the real assembly, a uniform velocity profile is applied at the inlet. The main focus is the temperature distribution and the maximum temperature in the heated region, which starts 660 mm (more than 2.5 times the wire pitch) downstream. This distance if sufficient for the flow to develop hydraulically, since the flow field is highly dominated by the geometry of the wire-wrapped rods. Figure 11 shows the velocity distribution (mean value = 1.8 m/s) at two axial positions in the unheated region. At both axial planes, the patters are similar, showing a swirling flow following the rotation of the wires. Some characteristic velocity magnitudes are 1.7 m/s at one side of the bundle and 2.4 m/s at the opposite side.

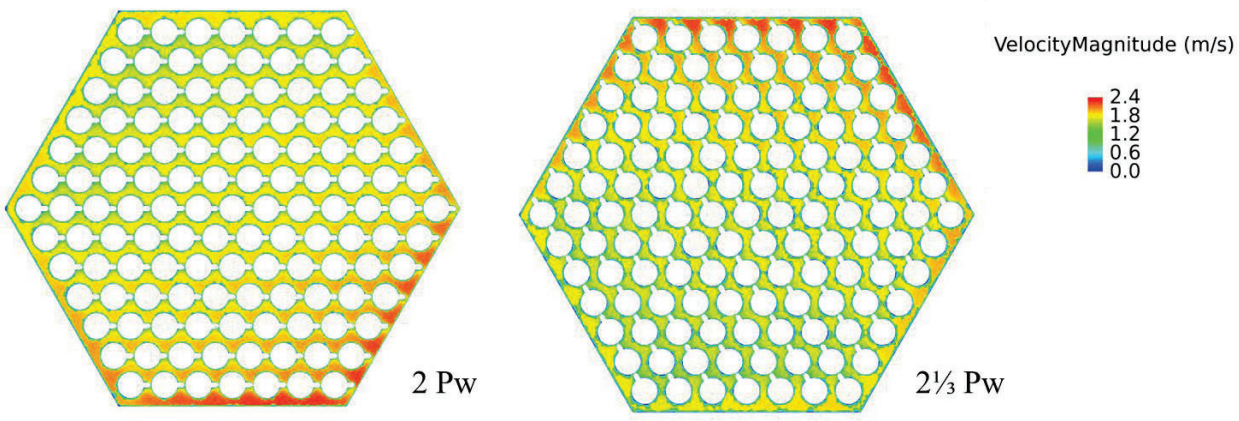


**Figure 11. Velocity magnitude at 2 and 2⅓ wire pitch from the inlet.**

The temperature distribution shown in Figure 12 indicates a hot region near the center rods and colder near the wrapper, in agreement with the experiments. This is due to the larger velocity near the wrapper, as shown by the velocity magnitude in the insets, and the adiabatic boundary condition applied at the wrapper. The indicated planes are at 1.8 and 2.15 wire pitches from the start of the heated section. Note the difference in scaling, which shows that the average bulk temperature is increased. The maximum temperature in the fuel assembly is 737 K (464°C), which is located in the center of the rod bundle near the end of the heated section. An overview of the temperature distribution is presented in Figure 13, confirming the hot LBE at the center and the colder LBE at the sides of the fuel assembly.

## 8. CONCLUSIONS

For the innovative MYRRHA reactor LBE is considered as the primary coolant. This work is focused on the assessment of the core fuel assemblies during nominal operation. This is a challenging study due to the limited amount of available experimental information and limitations of the current turbulence models for applications in liquid-metal flow in complex geometries. For that reason, this study includes both experimental and simulation activities in the framework of the European project SEARCH.

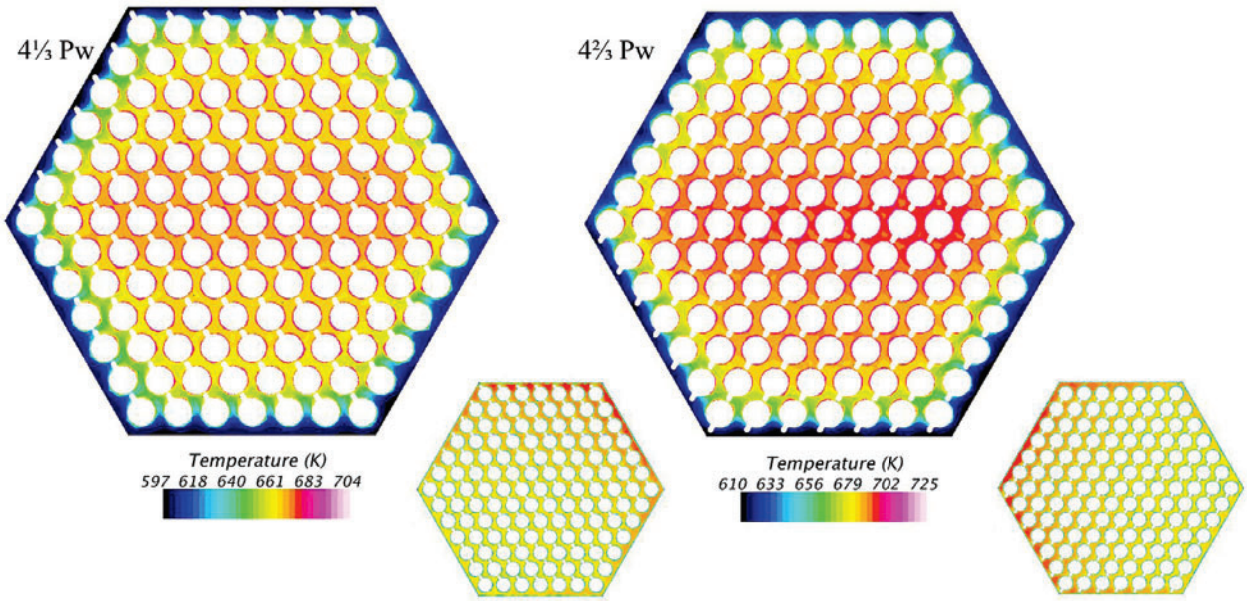


**Figure 12. Temperature at 4⅓ and 4⅔ wire pitch from the inlet.**


**Figure 13. Temperature distribution in the MYRRHA fuel assembly under nominal conditions.**

An experimental campaign at KIT-KALLA considers first-of-their-kind heated tests on a scaled mockup of the MYRRHA fuel assembly. For practical purposes, the size of the bundle is reduced from 127 to 19 and the heating elements are slightly larger. Nevertheless, the relevant P/D and H/D ratios are kept constant, as well as the Reynolds number and heat flux density. Thus, the geometry and the operating conditions are representative of the MYRRHA fuel assembly under nominal conditions. Detailed instrumentation is installed in the test section, providing temperature profiles at selected locations at the wall and the fluid, at three axial positions. The measurements present a high degree of reproducibility, and the results for one reference case are presented in detail in this work.

Large temperature differences are observed at each measurement level, as a consequence of the flow disturbances produced by the wire spacers. These profiles are studied in terms of $T-T_b$ and $T_w-T_f$, particularly around five selected sub-channels (A to E). A very good agreement is observed between the experimental data and the prediction of empirical correlations, particularly for the pressure difference. The experimental Nusselt number is best predicted by the most conservative correlation, by [12].

A computational approach is developed at NRG, implemented in the commercial code STAR-CCM+ and based on the SST k-ω turbulent model, with second order schemes. For practical purposes, the wire shape is approximated following a preliminary study on this effect. Two specific models are used.

First, considering the conjugate heat transfer in the solid structures (rods, wires), the reference experimental case is studied. The same general trends are observed within the simulations and the heat transfer compares well. As could be expected from literature, the pressure drop is slightly under predicted by both numerical simulations.

Second, considering only the fluid, the larger MYRRHA fuel assembly under nominal conditions is studied. The maximum temperature in the bundle are obtained, reaching up to 737K (464°C).

The combination of experiments and simulations provides a solid approach for the safety assessment of the MYRRHA fuel assembly. This work shall be continued, considering additional cases. Moreover, future activities shall be focused on non-nominal operating conditions.

## ACKNOWLEDGMENTS

The financial support of the European Union in the framework of the EU 7th framework project SEARCH, grant number 295736, is greatly appreciated. The authors also like to acknowledge the support of Markus Daubner and Frank Fellmoser (KIT) in the experimental campaign

## REFERENCES

1. G. Grötzbach. "Challenges in low-Prandtl number heat transfer simulation and modelling". *Nuclear Engineering and Design* **264**, pp. 41-55 (2013)
2. K. Mikityuk, "Heat transfer to liquid metal: Review of data and correlations for tube bundles", Nuclear Engineering and Design, 239, pp. 680 – 687 (2009)
3. W. Baumann, V. Casal, H. Hoffmann, R. Möller, K. Rust. "Brennelemente mit wendelförmigen Abstandshaltern für Schnelle Brutreaktoren", Kernforschungszentrum Karlsruhe, Technical report KFK-0768 (1968)
4. R. Collingham, V. Hill, J. Yatabe, W. Thorne, J. Chen, A. Bishop, "Development and results of an electrically-heated seven-pin bundle assembly for thermal-hydraulic testing in liquid metals", Liquid-metal heat transfer and fluid dynamics, New York, November 30, 1970, pp. 41-49 (1970)
5. M. Fontana, R. MacPherson, P. Gnadt, L. Parsly, J. Wantland, "Temperature distribution in the duct wall and at the exit of a 19-rod simulated LMFBR fuel assembly (FFM Bundle 2A) ", *Nuclear Technology*, **24**, pp. 176-200 (1974)
6. F. Engel, B. Minushkin, R. Atkins, R. Markley, "Characterization of heat transfer and temperature distributions in an electrically heated model of an LMFBR blanket assembly", *Nuclear Engineering and Design*, **62**, pp. 335 - 347 (1980)
7. F. Namekawa, K. Mawatari, A. Ito, N. Farukhi, "Buoyancy effects on wire-wrapped rod bundle heat transfer in an LMFBR fuel assembly", *AIChE Symposium Series*, **236**, pp. 128-133 (1984)
8. S. Chen, N. Todreas, N. Nguyen. "Evaluation of existing correlations for the prediction of pressure drop in wire-wrapped hexagonal array pin bundles". *Nuclear Engineering and Design* **267**, pp. 109-131 (2014)
9. S.-K. Cheng, N. Todreas. "Hydrodynamic models and correlations for bare and wire-wrapped hexagonal rod bundles. Bundle friction factors, subchannel friction factors and mixing parameters". *Nuclear Engineering and Design*, **92**, pp. 227 – 251 (1986).
10. P. Ushakov, , A. Zhukov, N. Matyukhin, "Heat transfer to liquid metals in regular arrays of fuel elements" High Temperature (USSR) **15**, pp. 1027-1033 (1978)
11. Handbook on Lead-Bismuth Eutectic alloy and Lead properties, materials compatibility, Thermal Hydraulics and Technologies, OECD, NEA No. 6195 (2007)

12. M. Kazimi, M. Carelli. “Clinch River Breeder Reactor Plant - Heat transfer correlation for analysis of CRBRP assemblies” *Westinghouse Electric Corporation*, Technical report CRBRP-ARD-0034 (1976)
13. D. De Bruyn et al., “The MYRRHA ADS project in Belgium enters the Front End Engineering Phase”, Proceedings of the 2014 International Congress on Advances in Nuclear Power Plants, Charlotte, NC, United States, 6-9 April 2014, American Nuclear Society, pp.646-654 (2014).
14. ESNII, “A contribution to the EU Low Carbon Energy Policy: Demonstration Programm for Fast Neutron - Concept paper”, Sustainable Nuclear Energy Technology Platform (2010).
15. F. Roelofs, V. Gopala, S. Jayaraju, A. Shams, E. Komen. “Review of Fuel Assembly and Pool Thermal Hydraulics for Fast Reactors”. *Nuclear Engineering and Design*, **265**, pp. 1205-1222 (2013)
16. J. Pacio, M. Daubner, F. Fellmoser, K. Litfin, L. Marocco, R. Stieglitz, S. Taufall, T. Wetzel. “Heavy-liquid metal heat transfer experiment in a 19-rod bundle with grid spacers”. *Nuclear Engineering and Design* **273**, pp. 33 - 46 (2014)
17. R. Möller, H. Tschöke. “Theoretische Untersuchungen zur Wandtemperaturmessung an simulierten Brennstäben für thermodynamische Experimente in Natrium”. Technical report KFK-1555, Kernforschungszentrum Karlsruhe (1972)
18. F. Roelofs, A. Shams, I. Otic, M. Böttcher, M. Duponcheel, Y. Bartosiewicz, D. Lakehal, E. Baglietto, S. Lardeau, X. Cheng, “Status and perspective of turbulence heat transfer modelling for the industrial application of liquid metal flows”. *Nuclear Engineering and Design* (2015) http://dx.doi.org/10.1016/j.nucengdes.2014.11.006.
19. V. Gopala, H. Doolaard, V. Sanna, F. Roelofs. “Detailed investigation of flow through wire-wrapped fuel assemblies using computational fluid dynamics”, THINS 2014 international workshop, Modena, Italy, January 2014
20. E. Merzari, P. Fischer, K. van Tichelen, S. Keijers, J. De Ridder, J. Degroote, J. Vierendeels, H. Doolaard, V.R. Gopala, F. Roelofs, “Benchmark exercise for fluid flow simulations in a liquid metal fast reactor fuel assembly”, *Nuclear Engineering and Design* (under review) (2015)
21. H.J. Doolaard, H.A. Bijleveld, V. Sanna, D. Rosa, V.R. Gopala. “Report on pre- and post-test analyses of the NACIE and THEADES experimental loops and assessment of the 127 pin MYRRHA Fuel Assembly”, EU FP7 SEARCH *Deliverable 2.8* (2015)
22. Roelofs F., Shams A., Otic I., Böttcher M., Duponcheel M., Bartosiewicz Y., Lakehal D., Baglietto E., Lardeau S., Cheng X., 2015. “Status and perspective of turbulence heat transfer modelling for the industrial application of liquid metal flows”, *Nuclear Engineering and Design*

## APPENDIX A

The physical properties of LBE considered in this work are listed in Table IV.

**Table IV. Physical properties of LBE, from [11]. T is the temperature in Kelvin.**

| Property | Formula | Uncertainty | At 300°C |
|---|---|---|---|
| **Density (ρ), kg m$^{-3}$** | 11096 - 1.3326 T | ≤0.8% | 10337 |
| **Heat capacity (cp), J kg$^{-1}$ K$^{-1}$** | 159 - 2.7210$^{-2}$ T + 7.12 10$^{-6}$ T$^2$ | ≤7.0% | 145.7 |
| **Th. conductivity (l), W m$^{-1}$ K$^{-1}$** | 3.61 + 1.517 10$^{-2}$ T - 1.741 10$^{-6}$ T$^2$ | ≤5.0% | 11.7 |
| **Viscosity (m), kg m$^{-1}$ s$^{-1}$** | 4.94 10$^{-4}$ exp(754.1/T) | ≤5.0% | 1.84 10$^{-3}$ |
| **Prandtl number (Pr), -** | $c_p \mu \lambda^{-1}$ | ? | 0.023 |